18 The Astrometric Error Budget

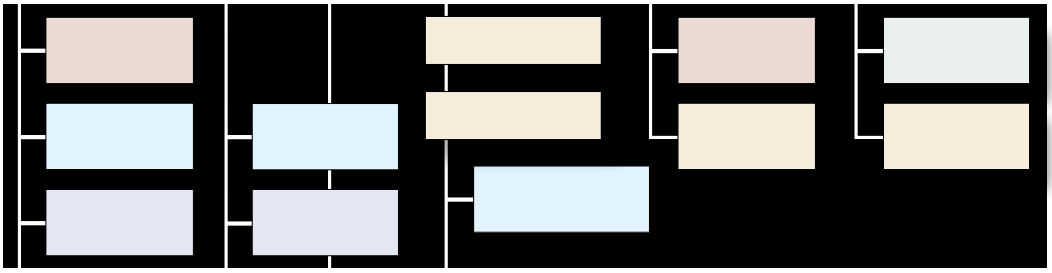

Bijan Nemati (JPL) and **Mauricio J. Morales** (JPL)

ABSTRACT

SIM Lite's performance is managed through the astrometric error budget. The astrometric error budget is designed to levy requirements on the various SIM Lite systems such as the metrology beam launchers, the astrometric beam combiners, and the delay lines. This performance model has been thoroughly validated using testbeds and more detailed models.

18.1 Introduction

Detecting the stellar wobble due to an Earth analog from a distance of 10 pc requires a per-visit astrometric accuracy of less than 1 μas. In Chapter 16 we saw that, with a 6 m baseline, this means that the external delay needs to be measured with a total error of less than 30 pm. Approximately half of this error is allocated to brightness-dependent errors, leaving only about 15 pm as the total allowable error in the science delay from all systematic sources. The dominant source of random errors is photon noise in the collected star light. Systematic errors arise from both extrinsic and instrument intrinsic sources.

SIM Lite's astrometric error budget (AEB) is a performance model designed to levy requirements and monitor the capability of the instrument in doing astrometry. It has received extensive testing and validation using testbeds and other models. In this chapter, we review the top-level structure of the AEB and discuss some of the more important error categories.

18.2 The Astrometric Error Budget

SIM Lite's AEB specifies the allowable error after a specified level of post-processing for each of two key observing scenarios: these are the grid and the narrow-angle scenarios. The grid scenario is a representation of a typical tile visit, including only the grid stars, while the narrow-angle (NA) scenario is designed to be a representation of a typical planet-finding visit. These two scenarios were chosen as drivers for the design because they are each key representatives of two different regimes of SIM Lite operations. Grid astrometry requires wide-angle operations and facilitates regularization and other essential calibrations of the instrument. Hence, it is the basis for all other astrometry. The search for exoplanets, on the other hand, is a key science objective and in many ways places the most demanding requirements on the instrument. Since the search for exoplanets is narrow angle in nature (less than one degree between any two stars measured), its error budget complements that of the wide-angle grid astrometry.

As with any form of astrometry, the final astrometric product is the result of extensive post-processing. The post-processing applies calibrations and combines all the measured quantities according to a detailed algorithm. Each observing scenario, whether searching for planets or measuring the astrometric grid, requires its own observation strategy and associated processing algorithm. These observing strategies aim to minimize the measurement error while at the same time also minimizing overall mission cost in terms of observation time.

Detailed observing scenarios and algorithms have been developed for SIM Lite's main observing modes. These have been tested extensively by modeling and have been validated in the various SIM Lite testbeds. Chapter 15 describes these observing scenarios in detail.

18.3 Grid AEB Top-Level Structure

The top-level grid error budget is shown in Figure 18-1. It is a performance model that captures the single-axis, mid-mission, grid star position error after the entire mission data set has been processed. Extensive mission observation and processing simulations have shown that the grid processing combines N_g separate measurements of each grid star to produce a grid with errors significantly less than the single-measurement error (note that we do not assume the errors scale as $1/\sqrt{N_g}$). The simulations predict that after the post-processing is complete, the mid-mission grid star position error is reduced by the "grid solution multiplier" of 0.25. The single-tile error is the position error per axis after only one tile of grid stars has been processed. It accounts for astrophysical errors including, in order of importance, stellar companions, stellar aberration, and gravitational perturbations.

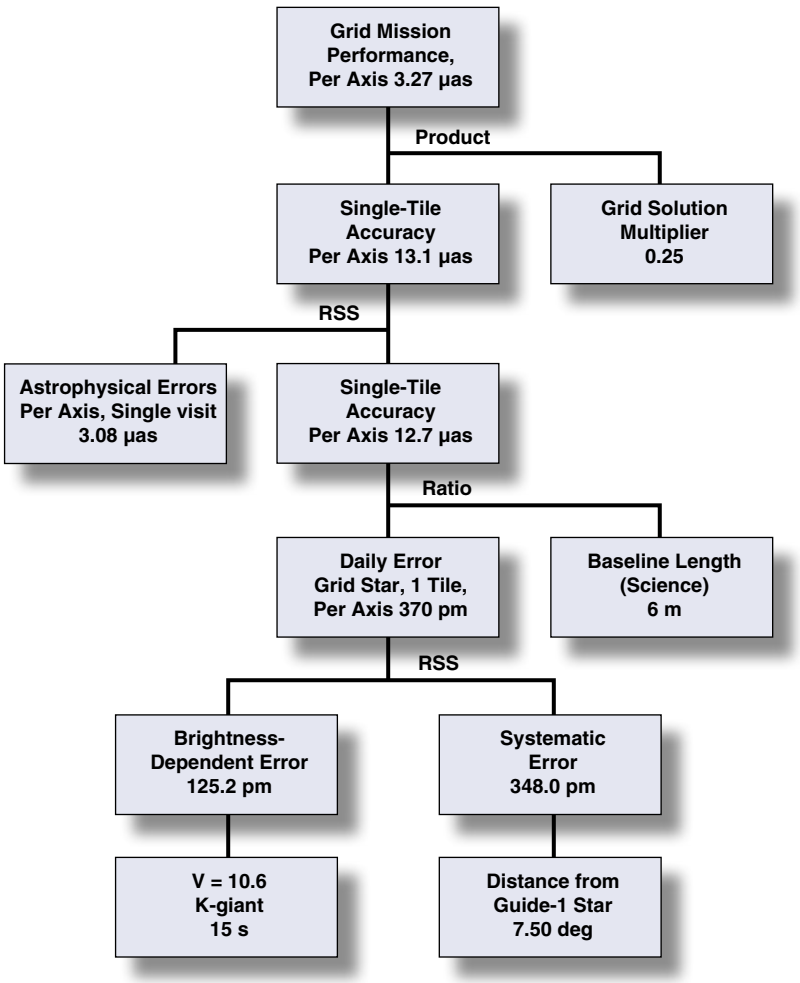

Figure 18-1. The top-level portion of the grid astrometric error budget is based on the end-of-mission performance in measuring grid star positions in each axis.

One level below, the error is expressed in pm of delay. Since the basic measurement of an astrometric interferometer is starlight delay, it is most convenient to specify instrument astrometric performance in units of allowable delay error. Instrument errors are divided into two major categories of brightness-dependent (random) errors and instrument systematic errors.

18.4 Narrow-Angle AEB Top-Level Structure

The top-level narrow-angle error budget is shown in Figure 18-2. Its performance metric is the single-visit, single-axis, effective single-measurement position error. To get the effective single-measurement error, the error budget assumes the target and reference star observations contribute equally to the differential astrometric error. Hence, it is set to equal the differential error divided by $\sqrt{2}$. The differential astrometric error includes contributions from astrophysical effects and non-ideal reference star geometry. One level below, the budget has two branches, one corresponding to errors from the target star and the other from the reference stars. Specific assumptions have to be made about the reference and target star brightness, spectral type, and observation durations. These, as mentioned above, are captured by the straw-man observing scenario. The breakdown below this level is similar to the grid error budget, with the branches being brightness-dependent and systematic errors.

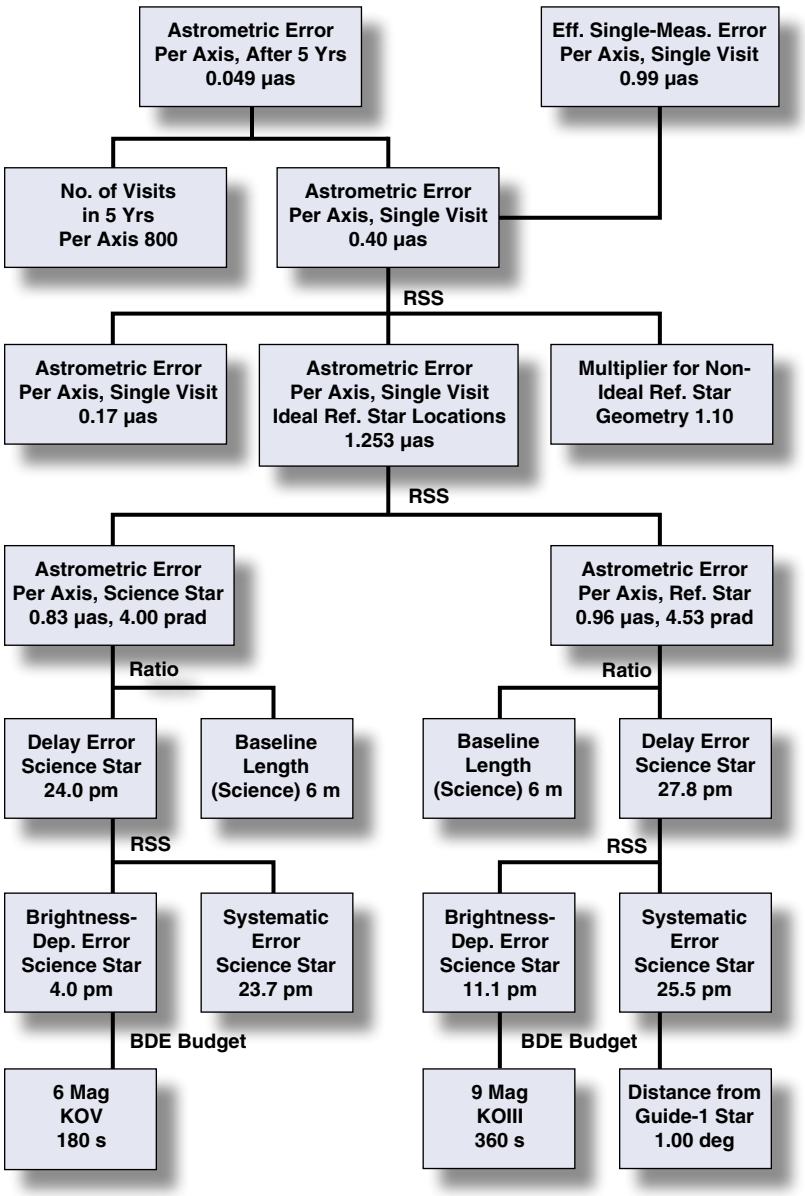

Figure 18-2. The top-level portion of the narrow-angle astrometric error budget is based on the effective single-visit, single-measurement error under a planet-finding scenario.

18.5 Brightness-Dependent Error

Brightness-dependent error (BDE) primarily arises from shot noise in the collected starlight, dark current in the detector, and read noise in the readout electronics. It is random in nature, and goes down with integration time. Figure 18-3 illustrates the important elements affecting BDEs.

In this figure, starlight from the two arms is combined, dispersed, and focused on the fringe detector. The light is converted to electrons according to the quantum efficiency of the detector. In SIM Lite, the fringe is formed temporally, as the delay is modulated. Since the fringe is dispersed across the detector, each pixel maps to a relatively narrow spectral channel.

Within each channel, the visibility of the fringe is given by:

$$V = \frac{I_{max} - I_{min}}{I_{max} + I_{min}} = \frac{a_0}{n_0} \qquad (1)$$

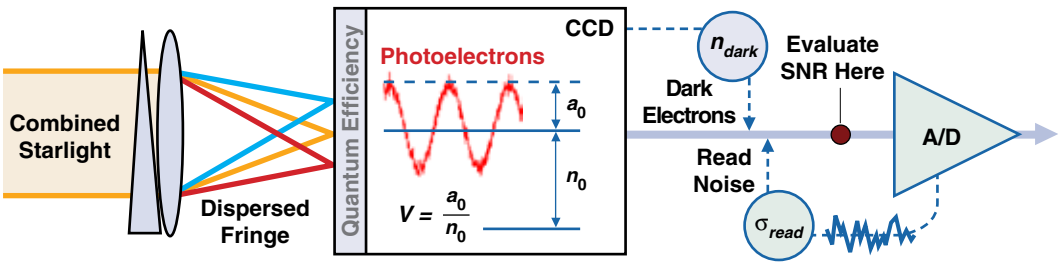

Figure 18-3. The brightness-dependent error fringe measurement is affected both by photon noise and detector noise.

where I_{min} and I_{max} are the minimum and maximum intensity in the fringe, respectively, and alternatively a_0 and n_0 are the "ac" and "dc" levels of the fringe. The phase is best estimated near a "zero crossing" of the fringe.

The phase error is given by the reciprocal of the fringe signal-to-noise ratio (SNR) near the zero crossing:

$$\delta\phi = \frac{1}{SNR} = \frac{\sqrt{n_0 + n_{dark} + \sigma_{read}^2}}{V n_0} \tag{2}$$

where n_{dark} is the accumulated dark current, in electrons, and σ_{read} is the read noise, again in electrons. The brightness-dependent error is simply the phase error converted into pathlength. Putting it all together, the full expression for the brightness dependent error within a spectral channel is given by:

$$\sigma_{BDE} = \frac{\lambda}{2\pi} \cdot (\gamma\, \delta\phi) = \frac{\lambda}{2\pi} \cdot \gamma \frac{\sqrt{n_0 + n_{dark} + \sigma_{read}^2}}{V n_0} \tag{3}$$

where λ is the mean wavelength within the spectral channel and γ is a correction factor for the fact that the fringe has to be sampled at a number of points, not just the (ideal) zero crossings, before a phase estimate is obtained. We note that, as expected, the error goes down with integration time.

The BDE is an important error and drives the instrument in many very important ways. A cursory glance at Equation (3) immediately shows that the BDE has a first-order dependence on visibility. Visibility is wavelength dependent and ranges from about 0.7 to 0.9 over most of the spectrum covered by the fringe detector. Many attributes of the combined beams affect the visibility, with the most important being relative static wavefront, jitter in pathlength difference or tilt difference, and mismatch in footprint, polarization, or amplitude. The visibility requirements thus drive the instrument to have diffraction-limited optics, nanometer-class pathlength control, and mas-class jitter control. The STB-3 testbed described in Chapter 19 has demonstrated control at levels better than these requirements on a flight-like structure.

The BDE's next strongest sensitivity is to n_0, the total collected number of photons. This drives the instrument towards maximizing the collecting area and optical throughput.

Finally, the BDE also places requirements on the allowed dark current and read noise. The fringe detector in SIM Lite is specified to have a read noise of less than five electrons per read and dark current less than 0.01 e-/pixel/sec. With proper electronics and thermal design, both of these performance requirements are straightforward to accomplish.

18.6 Instrument Systematic Errors

The instrument systematics portion of the SIM Lite AEB is shown in Figure 18-4. At the highest level, each of the primary sensors is represented: the science and Guide-1 interferometers, the Guide-2 telescope, and the external metrology system. The errors from each of these sensors can in general be considered independent. The exceptions are captured in a separate branch called "second-order errors" and will be described separately. A more detailed instrument model, which includes effects to the second order, has validated this simple breakdown structure for the errors.

Figure 18-4. SIM Lite's instrument systematics error budget has been tested and validated against the independently developed and more detailed SIM Lite instrument model. The grid example is shown here.

The values appearing in the boxes are the current best estimates of performance. The basis of most estimates ranges from actual performance measured in a prototype or testbed to engineering judgment based on previous work. As will be shown in Chapter 19, the algorithmic advances made alongside the

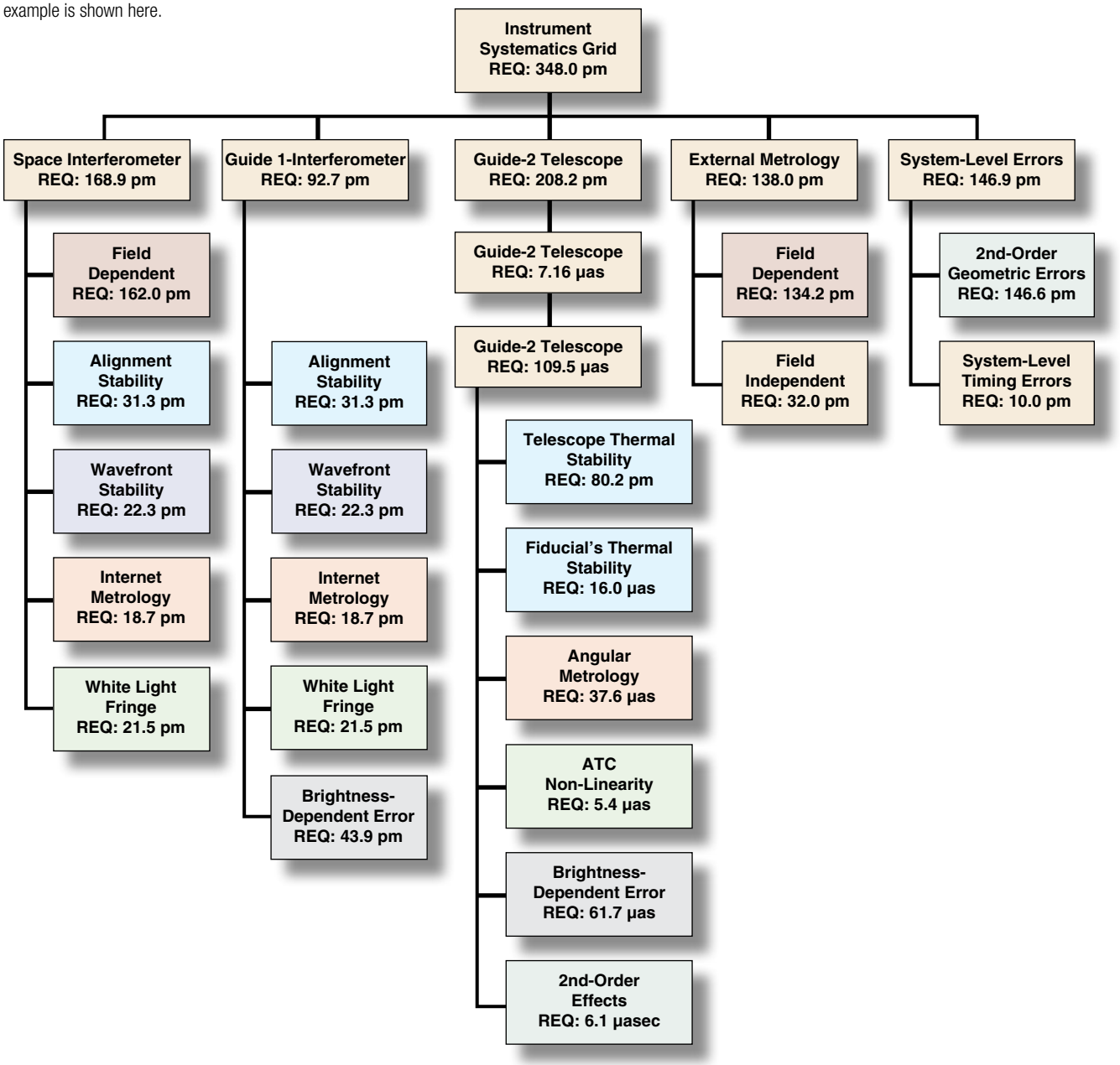

technology development have brought about a great deal of relaxation to the requirements at the hardware level. These algorithmic improvements usually fall into the categories of reduction and randomization of errors through strategic temporal programming of observations (such as chopping) and calibration of systematic effects using constrained fits to astrometric observations. The performance estimates in the error budget include the filtering effects of the processing algorithms.

18.6.1 Interferometer Errors

The science and Guide-1 interferometer systematic errors are similar, with the exception that the science interferometer has a siderostat which gives it a 15 degree FOR while the Guide-1 interferometer has a fixed collector. As a result, the entire category of field-dependent errors is absent for the Guide-1 interferometer. On the other hand, since the Guide-1 interferometer boresight is coincident with the center of the science FOR while the guide baseline is shorter than the science baseline, Guide-1 instrument errors are magnified by the ratio of the science baseline to the Guide-1 baseline. This makes Guide-1 requirements every bit as stringent as the science interferometer requirements.

We discuss the interferometer errors organized within the broader categories of the fundamental measurements: white light fringe delay, internal delay, and the baseline vector. Detailed mission modeling has verified that completeness at the topmost level is assured if these three fundamental measurements are captured.

18.6.2 Measuring the White Light Fringe

The total (internal plus external) optical pathlength difference (OPD) is given by the white light fringe phase. In SIM Lite, the fringe is temporal in nature, being observable by modulating the pathlength. It is also spectrally dispersed across a number of pixels using a prism, shown in Figure 18-5. The fringe phase is obtained by modulating the pathlength and recording the resulting photoelectron counts at each of a number of spectral channels. The white light fringe on the “minus” or “dark” side of the beam splitter is shown in Figure 18-5. The fringe on the other side would be bright at zero OPD, and is also used.

Pathlength modulation for measuring fringe phase is used in a number of commercial interferometers. None of the commercial interferometers have accuracy below 100 pm. By using a pm-accurate metrology system to measure the position of the pathlength modulator and using that information along with the CCD measurements in a least-squares estimate of the complex visibility, SIM Lite eliminates the largest and most common error in pathlength modulation interferometry.

At the subnanometer level, two types of systematic errors remain. Both of them are related to the fact that we are measuring the optical phase of a white light fringe rather than a monochromatic light source’s fringe. As the interferometer is pointed at different stars with different spectral energy distributions, two sources of errors can arise. They are (1) dispersion and polarization in the optics, and (2) changes in the effective wavelength of the light. SIM Lite addresses these errors by calibrating the dispersion curve daily and measuring the spectrum of each observed star once during the mission. This approach is currently being refined using a testbed called the Spectral Calibration Development Unit.

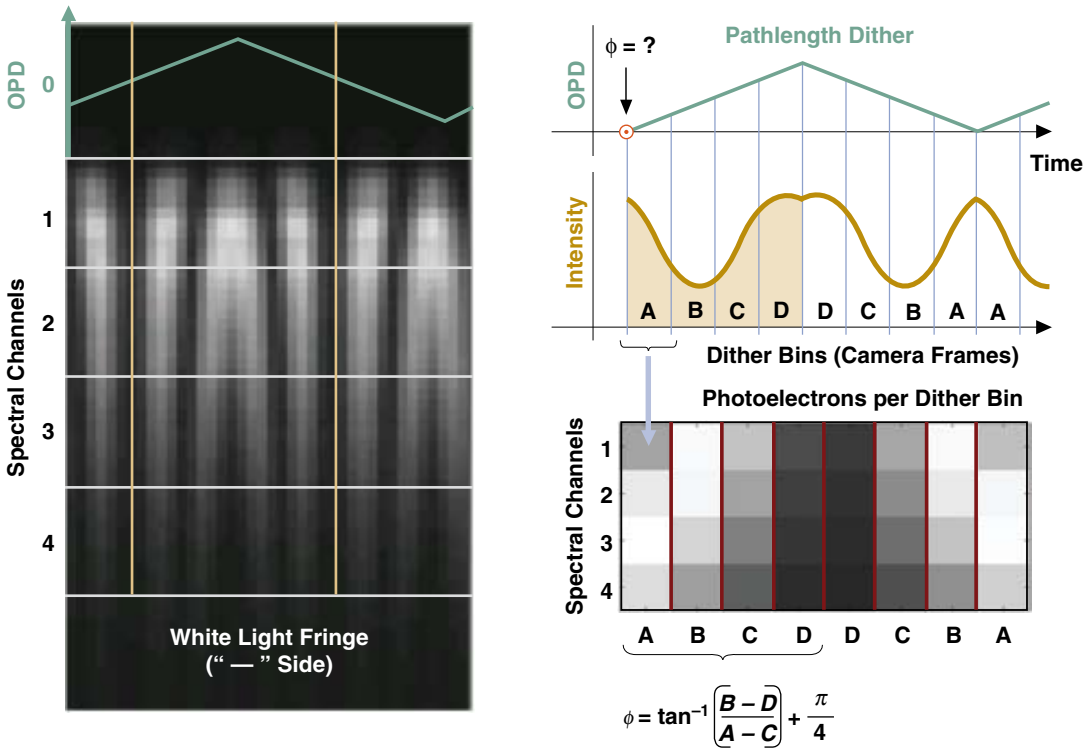

Figure 18-5. Phase estimation using dithering is illustrated here; the response of four spectral channels is shown as the delay is dithered. The spectrally dispersed white light fringe is on the left. A, B, C, D are the integrated detector counts during each temporal quadrant of pathlength dither. With the aid of precision metrology, SIM Lite has successfully demonstrated pm-class fringe delay estimation.

18.6.3 Measuring the Internal Delay

The starlight internal delay is measured using the internal metrology system. An infrared laser beam originates from a beam launcher and is separated into two beams by the beam combiner/splitter. The two beams make round-trip journeys to the two double corner cubes (DCCs, one at each siderostat) and return to the beam launcher with phase delay, which measures internal pathlength difference (Figure 18-6).The footprints of the two metrology beams are within the annular footprint of the starlight beam.

In the error budget, any deviation between what the starlight experiences and what the metrology measures is book-kept under internal metrology error. Since the metrology footprint is a small central region inside the annular starlight footprint, differences can arise between the two, leading to errors. For example, at the siderostat, the starlight bounces off the annular mirror while the internal metrology beam only senses the DCC mounted at the center. When the siderostat, with its DCC, is turned from one star to another, an error proportional to the offset between the vertex of the corner cube and the surface of the siderostat arises. This error will depend on the siderostat look angle within its FOR, and is hence called a field-dependent error (Figure 18-7).

Another source of field-dependent error lies within the optical delay line (ODL), which is the system that changes the internal delay to match pathlengths. As the instrument switches from star to star within its FOR, the delay can change by as much as 2 m. As the ODL compensates for this, the imperfections in the ODL mechanical structure will induce micron-level lateral motion (beam walk) of the light on the optics. Since the footprints of metrology and starlight are different, imperfections in the optics cause different delay changes between the two, leading to a field-dependent error.

The mitigation of these field-dependent errors requires a combination of tight tolerances on opto-mechanical parts and calibration of residual requirements using star observations. This approach has been validated using the Microarcsecond Metrology (MAM) testbed and SIM Lite mission modeling.

Alignment instability in the metrology beam can cause beam-walk errors as the diffracted metrology beam walks across the optics. Beam-walk errors have been tested both in the MAM testbed and the diffraction testbed. The results from these testbeds indicate that the beam-walk errors in SIM Lite are controllable to within error budget allocations.

Wavefront instability, mostly driven by thermal changes anywhere along the optical train, can translate into an effective metrology error, again due to the difference in the starlight and metrology footprints. SIM Lite's Thermo-Opto-Mechanical (TOM) testbed (described in Chapter 19) has demonstrated that, thanks to the thermal mass of the components involved, the thermal environment is sufficiently quiescent to keep the errors within the allocations.

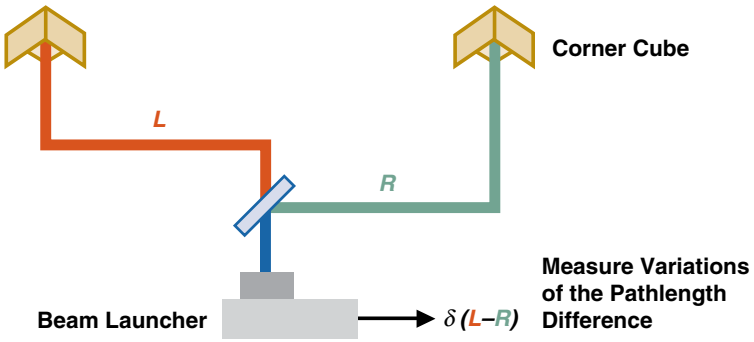

Figure 18-6. The internal metrology gauge monitors the changes in the left-right optical pathlength difference in the interferometer at the pm level.

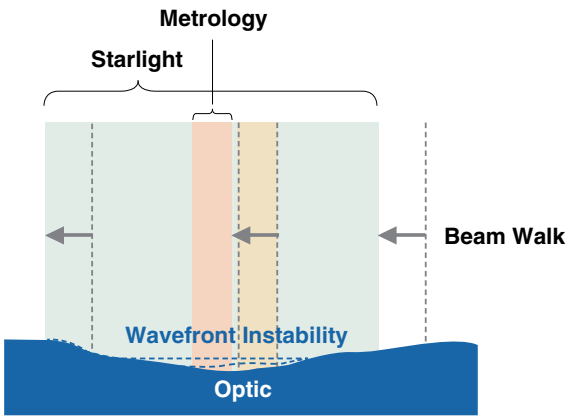

Figure 18-7. There are two ways metrology can be in error relative to starlight. Figure errors in the optics can result in sensitivity to beamwalk. Here, the starlight and metrology are "walking" together across the optic, resulting in a net OPD error. Alternatively, a change in the surface figure ("wavefront instability") can cause a difference between the metrology and starlight. These effects have been fully tested in a number of SIM Lite testbeds and shown to be controllable to within requirements.

18.6.4 Guide-2 Telescope Errors

Another branch of the instrument systematics error budget (see Figure 18-4) is the Guide-2 telescope (G2T) branch. Converting the allocation to G2T's native units of attitude knowledge accuracy, the requirements on G2T are 50 and 100 μas for the NA and Grid scenarios, respectively. To get the level of centroiding accuracy needed to support these requirements, a pointing loop is used to maintain the line of sight (LOS) of the telescope on the "sweet spot" of the angle tracking camera (essentially the cross-hairs formed by specific pixel boundaries). Siderostat angular motions required to fix the star image on the angle tracking camera (ATC) are monitored using an angular metrology system. Angular metrology operates in a manner similar to internal metrology, except that it uses more beams so that it can perceive tip and tilt.

Ideally, G2T measures the rotation of the external metrology truss relative to inertial space. To make this tie, the telescope is mounted on a bench with fiducials that are monitored by external metrology beams. G2T's most important source of systematic error is thermally induced deformations. These deformations are broken down into two categories: the internal deformations of the telescope optics and motions of the fiducials with respect to the telescope.

It is useful to consider an example. If the thermal gradients induce a relative motion between the ATC and the siderostat, the star image would move in the ATC and the pointing loop would promptly rotate the siderostat to bring the image back to the nominal spot. At the same time, the angular metrology measurement would sense the correction and indicate a rotation relative to the star. This would be incorrectly perceived as an inertial rotation of the instrument.

The G2T error budget also includes the errors in measuring the centroid in the ATC. These include photon noise as well as nonlinearities in the centroiding algorithm arising from the finite sampling of the image by the CCD. These errors are minimized by driving the image to the "sweet spot" as mentioned before. Additionally, the G2T error budget includes the errors in measuring the tip/tilt of the siderostat with metrology beams. These include errors associated with knowledge of instrument geometry and metrology gauge errors.

Because the thermal errors are expected to be the largest contributors to the G2T errors, they have been given the highest allocation. These allocations were made consistent with the thermal deformations expected on orbit, using thermal models of SIM Lite under flight-like conditions.

To demonstrate that SIM Lite can meet these requirements, a new testbed called G2T has been built and is currently in operation. The testbed and the initial results are discussed in Chapter 19. So far, the results indicate that all the G2T requirements can be solidly met.

18.6.5 External Metrology Errors

All relative displacements between SIM Lite fiducials are measured using the external metrology system. The system is composed of beam launchers interposed between the fiducials, monitoring in each case a one-dimensional length. Each beam launcher is a miniature heterodyne laser interferometer with an accuracy of a few pm. Elements of a single link are shown in Figure 18-8.

External metrology errors are generally grouped into two main categories. These are one-dimensional gauge (field-independent) errors and field-dependent errors.

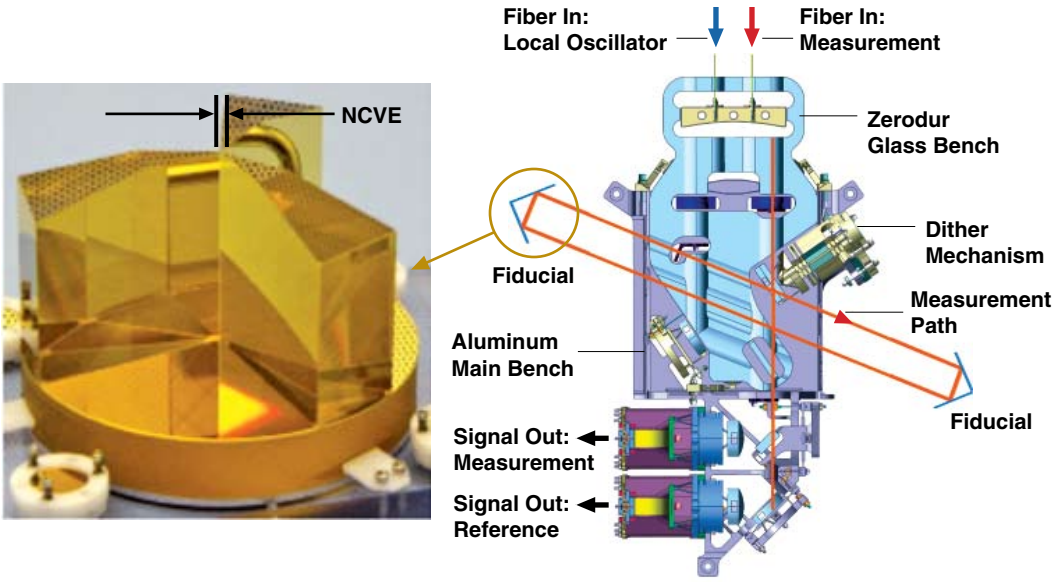

Figure 18-8. External metrology measures the distances between fiducials such as the double corner cube (DCC, left) using beam launchers (right). Noncommon vertex error (NCVE) is the distance between the two vertices of a DCC.

Field-independent errors primarily include gauge errors arising from crosstalk between laser metrology signals, thermal deformations within each beam launcher, alignment errors, and finite SNR in the detected laser signal. The metrology truss solution requires a micron-class survey of the instrument. This is done using beam launchers in two-color interferometry mode, which is dubbed "absolute metrology." Errors in the absolute metrology survey are also book-kept under field-independent errors.

As the siderostat with its DCC turns from star to star, the external metrology system incurs field-dependent errors due to a number of effects. First, we note that each fiducial is a multiple corner cube constructed in a way that the noncommon vertex error (NCVE, Figure 18-8) between its component corner cubes is as small as possible (less than a few microns). Even at this level, the noncommonality of the vertices in each DCC results in geometrical errors in the truss. Also, reflection phase shifts will be different on the different metrology beams that interrogate a given DCC. These beams will also be "walking" on the corner cubes. Any surface errors coupled with this beam walk result in errors. Finally, corner cube dihedral errors (deviation from orthogonality) cause additional field dependent errors.

SIM Lite's external metrology testbed, described in Chapter 19, was dedicated to demonstrating all of the technological aspects associated with external metrology. The results, discussed in Chapter 19, show that the technology to meet these external metrology requirements is at hand.

18.6.6 Second-Order Errors

The final branch to be discussed in the instrument systematics error budget concerns second-order errors. There are seven important second-order effects, and they are typically the product of a knowledge or measurement error and some motion. Figure 18-9 indicates all the second-order effects and highlights the ones that are significant.

They are all essentially residual errors that are beyond the reach of further calibration and enter into the astrometric measurement without further suppression. One example is the second-order error arising from the attitude control system (ACS) error (a motion) coupling with error in absolute metrology.

As mentioned in Chapter 16, by knowing the truss geometry and the measured ACS motion using the guide instruments, the science delay can be corrected for the science baseline motion. An error in the absolute metrology results in an error in the truss geometry knowledge, and hence an error in the corrected science delay.

This and all such errors are controlled by placing tight requirements on the motions in question and on the knowledge or measurement errors. These errors have been studied using instrument modeling and in testbeds, and their impact has been demonstrated to be tolerable.

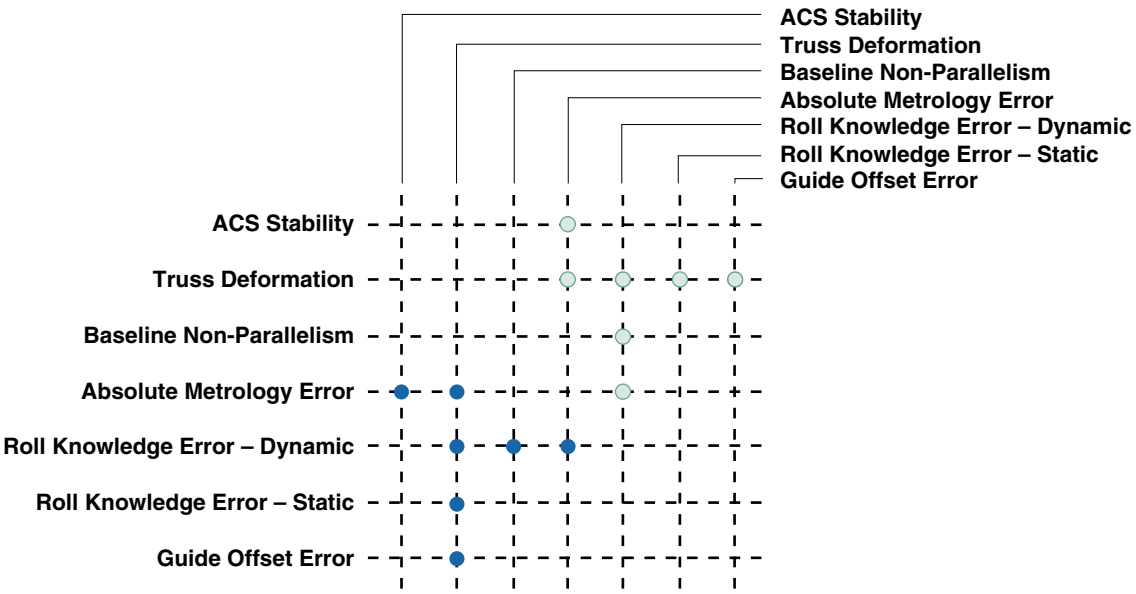

Figure 18-9. Second-order instrument systematics errors involve a motion coupled with a knowledge or calibration error.